Inorganic Chemistry
Article
Cite This: Inorg. Chem. 2019, 58, 14112−14119
pubs.acs.org/IC

Stability of Solid Uranyl Peroxides under Irradiation

Melissa Fairley,[†] Nicholas M. Myers,[†] Jennifer E. S. Szymanowski,[‡] Ginger E. Sigmon,[‡] Peter C. Burns,[‡,∥] and Jay A. LaVerne*[,†,§]

[†]Radiation Laboratory, University of Notre Dame, Notre Dame, Indiana 46556, United States
[‡]Department of Civil and Environmental Engineering and Earth Sciences, University of Notre Dame, Notre Dame, Indiana 46556, United States
[§]Department of Physics, University of Notre Dame, Notre Dame, Indiana 46556, United States
[∥]Department of Chemistry and Biochemistry, University of Notre Dame, Notre Dame, Indiana 46556, United States

Supporting Information

ABSTRACT: The effects of radiation on a variety of uranyl peroxide compounds were examined using γ-rays and 5 MeV He ions, the latter to simulate α-particles. The studied materials were studtite, $[(UO_2)(O_2)(H_2O)_2](H_2O)_2$, the salt of the U_{60} uranyl peroxide cage cluster, $Li_{44}K_{16}[(UO_2)(O_2)(OH)]_{60}\cdot 255H_2O$, the salt of $U_{60}Ox_{30}$ uranyl peroxide oxalate cage cluster, $Li_{12}K_{48}[\{(UO_2)(O_2)\}_{60}(C_2O_4)_{30}]\cdot nH_2O$, and the salt of the $U_{24}Pp_{12}$ (Pp = pyrophosphate) uranyl peroxide pyrophosphate cage cluster, $Li_{24}Na_{24}[(UO_2)_{24}(O_2)_{24}(P_2O_7)_{12}]\cdot 120H_2O$. Irradiated powders were characterized using powder X-ray diffraction, Raman spectroscopy, infrared spectroscopy, X-ray photoelectron spectroscopy, and UV−vis spectroscopy. A weakening of the uranyl bonds of U_{60} was found while studtite, $U_{60}Ox_{30}$, and $U_{24}Pp_{12}$ were relatively stable to γ-irradiation. Studtite and U_{60} are the most affected by α-irradiation forming an amorphous uranyl peroxide as characterized by Raman spectroscopy and powder X-ray diffraction while $U_{60}Ox_{30}$ and $U_{24}Pp_{12}$ show minor signs of the formation of an amorphous uranyl peroxide.

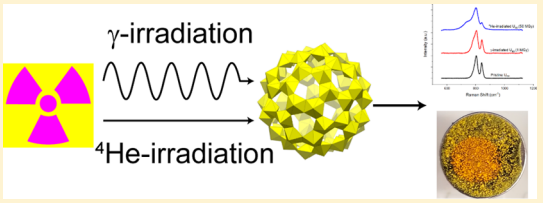

INTRODUCTION

Water that interacts with radioactive wastes may contain significant quantities of hydrogen peroxide produce by radiolysis. Alteration of uranium-rich nuclear waste in contact with such water can result in formation of uranyl peroxides with diverse compositions and structures.[1−4] Combination of uranyl ions and hydrogen peroxide in aqueous solutions with pH less than about 9 often results in precipitation of studtite, $[(UO_2)(O_2)(H_2O)_2](H_2O)_2$,[5] which is commonly produced during uranium processing owing to its low aqueous solubility. In contrast, in alkaline aqueous solutions uranyl ions readily combine with peroxide to produce an extensive and complex family of nanoscale uranyl peroxide cage clusters, the salts of which are very soluble in water.[4,6−8] Uranyl peroxide cages have potential applications in nuclear fuel cycles, specifically separation and purification of uranium on the front-end and back-end of the cycle as well as a possible role in the transport of actinides in the environment.[9] The separation of uranyl peroxide clusters from solutions derived by dissolving simulated spent nuclear fuel[10] and aqueous solutions was recently demonstrated using ultrafiltration.[11]

The first mention of a uranium peroxide compound in the literature appeared in 1877.[12] By 1950 $[(UO_2)(O_2)(H_2O)_2](H_2O)_2$ and $[(UO_2)(O_2)(H_2O)_2]$ were reasonably well-characterized,[13] although the structure for $[(UO_2)(O_2)(H_2O)_2](H_2O)_2$ was only determined in 2003.[14] These two compounds occur as minerals, with the tetrahydrate named studtite in 1947[15] and the dihydrate metastudtite in 1983.[16] The yellowcake produced from modern *in situ* uranium mining is usually a mixture of uranyl peroxides and oxides that result from heat treatment of studtite. Uranyl peroxide hydrates dehydrate above 200 °C to form an X-ray amorphous compound with approximate composition U_2O_7 that reacts with water to produce oxygen gas.[17,18] This compound likely contributed to accidents resulting from pressurized drums of yellowcake in the USA and Canada.[19] It is also known that electron-beam irradiation can amorphize studtite and meta-studtite under vacuum, and with continued irradiation, UO_2 uraninite nanocrystals may form.[20]

The first uranyl peroxide cage cluster was discovered in 2005,[6] and more than 65 uranyl peroxide clusters have since been reported. They contain from 16 to 124 uranyl ions and have diameters ranging up to 4 nm.[7] Uranyl peroxide polyhedra self-assemble in alkaline aqueous solution under ambient conditions.[7,21] Although peroxide is an essential component of this family of nanomaterials, structural and chemical complexity is enhanced by incorporation of several other uranyl-bridging ligands including hydroxyl, nitrate, pyrophosphate, and oxalate.[7] The oxygen atoms of the roughly linear $(UO_2)^{2+}$ uranyl ion stabilize the cage clusters both on the inside and outside, as these strongly bound atoms are relatively unreactive.

Received: July 17, 2019
Published: September 26, 2019

DOI: 10.1021/acs.inorgchem.9b02132
Inorg. Chem. 2019, 58, 14112−14119

Here we select four uranyl peroxide compounds for study under intense γ-irradiation and He ion irradiation and characterize the starting and irradiated materials using a combination of powder X-ray diffraction (PXRD), Raman spectroscopy, infrared (IR) and UV−vis spectroscopy, and X-ray photoelectron spectroscopy (XPS). The first of these is studtite, $[(UO_2)(O_2)(H_2O)_2](H_2O)_2$, the structure of which contains infinite chains of uranyl hexagonal bipyramids in which adjacent uranyl ions are bridged by bidentate peroxide.[14] The chains are linked into the crystal structure through H bonding involving interstitial H_2O and H_2O coordinated to the uranyl ions.

Three of the compounds selected for study here are salts of nanoscale uranyl peroxide cage clusters. The salt of U_{60}, $Li_{44}K_{16}[(UO_2)(O_2)(OH)]_{60}\cdot 255H_2O$, contains cages built from 60 uranyl ions with peroxide and hydroxyl bridging the uranyl ions and has a fullerene topology identical to C_{60}.[22−25] The stability of U_{60} has been studied in different environments and was determined to persist in high-pressure (17.4 GPa)[26] conditions as well as environmentally relevant conditions with goethite and hematite.[27,28] The salt of $U_{60}Ox_{30}$ uranyl peroxide oxalate cage clusters, $Li_{12}K_{48}[\{(UO_2)(O_2)\}_{60}(C_2O_4)_{30}]\cdot nH_2O$, contains cage clusters derived from U_{60} by replacing 30 pairs of hydroxyl groups with 30 oxalate ligands.[29−31] The salt of $U_{24}Pp_{12}$ (Pp = pyrophosphate) uranyl peroxide pyrophosphate cage clusters, $Li_{24}Na_{24}[(UO_2)_{24}(O_2)_{24}(P_2O_7)_{12}]\cdot 120H_2O$, contains cages composed of 24 uranyl polyhedra arranged into six uranyl peroxide tetramers. These tetramers are connected by bridging peroxo ligands and are cross-linked by Pp ligands.[32,33] The terminal oxygen atoms of the phosphate groups were determined to be unprotonated using single crystal neutron diffraction studies and participate in hydrogen bonding with nearby H_2O groups.[34]

EXPERIMENTAL SECTION

Sample Preparation and Analysis. Uranyl peroxide compounds were synthesized following previously reported methods.[14,23,31,32] The uranyl peroxide solids were analyzed before and after irradiation using Raman spectroscopy, XPS, IR spectroscopy, UV−vis spectroscopy, and PXRD.

PXRD measurements of studtite were collected using a Bruker D8 Advance Davinci powder X-ray diffractometer with a Cu Kα X-ray source. Scans were taken over a range of 7−50° 2θ while the sample was rotated at 15 rpm.

Raman spectroscopy measurements were taken using a Renishaw inVia Raman instrument. In our configuration, the estimated spot size is 10 μm and a 785 nm excitation laser was used for all compounds. Static scans had a laser power of 0.5%, 15 accumulations, and 1 s exposures while the extended scans were set to 0.1%, 10 accumulations, and 10 s exposures. Cosmic ray removal was done for all Raman scans. Raman spectra were fitted using OriginPro and Lorentzian functions. The inverse of the second derivative was used to identify hidden spectral bands.[35]

Infrared spectroscopy for γ-irradiated samples was performed using a Bruker Vortex 70 instrument. All uranyl compounds were mixed with KBr prior to collection. The spectral range collected was 400−4000 cm^{-1}. For He ion irradiated samples, IR was measured using a Bruker Lumos FT-IR in the attenuated total reflectance (ATR) mode. All IR measurements of He ion irradiated samples were collected directly from the irradiated SEM stub. The spectral range collected was from 600 to 3998 cm^{-1}.

XPS was performed on a PHI VersaProbe II X-ray photoelectron spectrometer equipped with a monochromatic Al Kα X-ray source. Wide survey scans over the binding range of 1486−0 eV were collected using a pass energy of 187.85 eV. High-resolution scans were taken of each element of interest with a pass energy of 23.5 eV. The estimated sample spot size was 100−200 μm in diameter and 10 nm in sampling depth. Data analysis was completed using PHI Multipak, and the energy scale was calibrated by setting the main carbon peak (C−C) to 285 eV.

UV−vis spectra were collected on a Jasco V-670 UV−vis−NIR spectrometer. Spectra of polycrystalline powders were collected using an integrating sphere from 200 to 800 nm.

Irradiation. Irradiations with γ-rays were performed using a self-enclosed Shepherd ^{60}Co source at the University of Notre Dame Radiation Laboratory. The dose rate determined by Fricke dosimetry as of January 2019 was 88.4 Gy/min. Polycrystalline powders were degassed using freeze−thaw techniques and flame-sealed in Pyrex tubes (1 cm diameter × 10 cm) for radiolysis. For α-irradiations, 5 MeV He ions were applied using the 9S Accelerator of the Nuclear Science Laboratory at the University of Notre Dame with a beam current of about 10 nA. Absolute dosimetry was performed by combining the incident energy with the integrated beam current. The beam diameter was 0.635 cm with a penetration of about 12 μm. Argon was flowed across the sample interface to reduce any oxygen interactions and to keep the sample at ambient conditions. Irradiation times were about 2 h, and no sample heating was observed. Uranyl peroxide samples for α-irradiation were prepared by depositing polycrystalline powder on SEM stubs using carbon tape. Typical doses for γ-irradiation were 1 MGy while that for He ion irradiation was 50 MGy.

RESULTS AND DISCUSSION

PXRD was used as an initial characterization tool to determine structural changes that occurred in the bulk sample during radiation. The salts of uranyl peroxide clusters such as U_{60}, $U_{60}Ox_{30}$, and $U_{24}Pp_{12}$ do not diffract well upon removal from the mother liquor and grinding because the crystallinity is impacted by dehydration. Therefore, only studtite was analyzed using PXRD. The PXRD patterns of studtite for the pristine and γ-irradiated samples are very similar (Figure 1). A

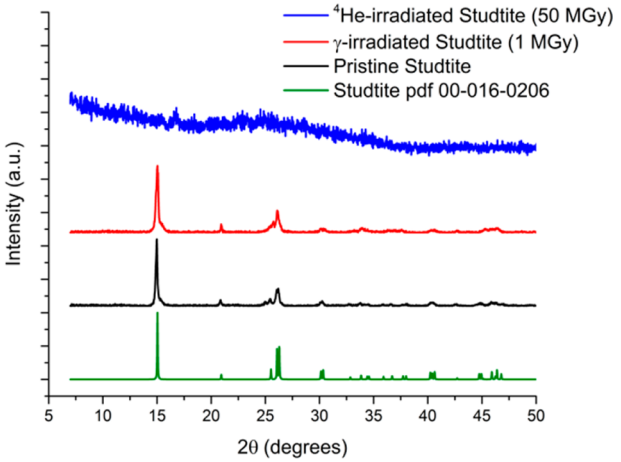

Figure 1. PXRD pattern of studtite PDF 00-016-0206 (green), pristine studtite (black), γ-irradiated studtite (red), and He ion irradiated studtite (blue).

subtle broadening of the peaks is observed after γ-irradiation, which is indicative of changes in the coherent domain of scattering or crystallinity. After He ion irradiation to 50 MGy, the material becomes amorphous with a broad peak ranging from approximately 20° to 35° 2θ.

Raman spectroscopy was used to probe the chemical changes of each of the compounds under study due to radiation exposure and emphasized the spectral window that encompasses the uranyl bonds and bridging peroxo groups

DOI: 10.1021/acs.inorgchem.9b02132
Inorg. Chem. 2019, 58, 14112−14119

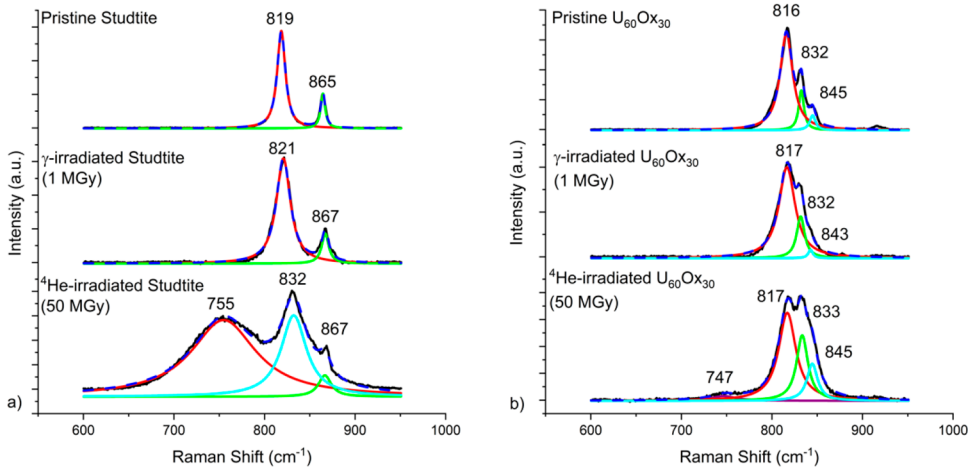

Figure 2. Deconvolution of the 600−950 cm^{-1} region of the Raman spectra of (a) pristine studtite (top), γ-irradiated studtite (middle), and He ion irradiated studtite (bottom). (b) Pristine salt of $U_{60}Ox_{30}$ (top), γ-irradiated salt of $U_{60}Ox_{30}$ (middle), and He ion irradiated salt of $U_{60}Ox_{30}$ (bottom). The black line is the raw data while the blue dotted line corresponds to the fitted sum.

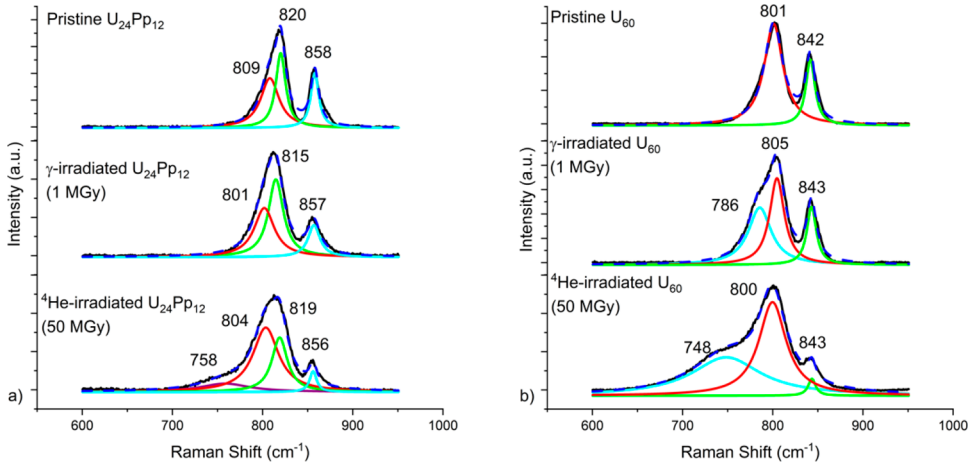

Figure 3. Deconvolution of the 600−950 cm^{-1} region of the Raman spectra of (a) pristine salt of $U_{24}Pp_{12}$ (top), γ-irradiated salt of $U_{24}Pp_{12}$ (middle), and He ion irradiated salt of $U_{24}Pp_{12}$ (bottom). (b) Pristine salt of U_{60} (top), γ-irradiated salt of U60 (middle), and He ion irradiated salt of U_{60} (bottom). The black line is the raw data while the blue dotted line corresponds to the fitted sum.

(700−950 cm^{-1}). Generally for the cluster salts, bands in the range of 800−820 cm^{-1} are assigned to the symmetric uranyl stretch (O═U═O), while the bands in the range of 820−850 cm^{-1} are assigned to the symmetric stretch of the peroxo O−O group.[36] For studtite, the peak at approximately 865 cm^{-1} is assigned to the symmetric stretch of the peroxo group.[37] When comparing the spectra of the pristine and γ-irradiated samples of studtite and $U_{60}Ox_{30}$, the most noticeable difference is the broadening of the Raman peaks in the spectra of the irradiated samples (Figure 2). Fitting of the uranyl and peroxo bands indicates that the full width at half-maximum (fwhm) of both bond stretches increases after γ-irradiation for all compounds examined with the exception of the $U_{60}Ox_{30}$ peroxo band at 843 cm^{-1} (Tables S1−S4). The samples also produce significant fluorescence in the Raman spectra after γ-irradiation. Both of these results indicate a partial loss in crystallinity of all four compounds under study due to γ-irradiation. The spectrum of the salt of the $U_{24}Pp_{12}$ cluster also reveals a large decrease in the intensity of the bridging peroxo peak at approximately ∼857 cm^{-1} (Figure 3a). A larger change is seen with the γ-irradiation of U_{60} represented in Figure 3b. Deconvolution of the peaks in the range of 700−950 cm^{-1} reveals a new peak at 786 cm^{-1} that is present only after γ-irradiation. This red-shift of the uranyl band at ∼800 cm^{-1} indicates lengthening and weakening of the uranyl bond.[35,38] A change in the chemical environment of the uranyl ion such as addition of a peroxide equatorial ligand made available by the breakdown of U_{60} or development of stronger cation−uranyl interactions is occurring.

Studtite and U_{60} undergo significant changes due to He ion irradiation. During the He ion irradiation, the studtite sample dehydrates from studtite to metastudtite. This transition is indicated by the shift of the uranyl peak in the Raman spectra from approximately 820 to 830 cm^{-1} in Figure 2a.[37] The Raman spectral peaks of studtite substantially broaden, and a new broad peak develops at 755 cm^{-1} (Figure 2a). This peak suggests the formation of a new uranium species due to the He ion irradiation. In the spectrum of the salt of U_{60}, the bridging peroxo peak at ∼843 cm^{-1} decreases a substantial amount and new broad peak appears at ∼748 cm^{-1} that is similar to that observed for the studtite sample (Figure 3b). The original uranyl band at ∼800 cm^{-1} is still present in the spectrum of the He ion irradiated sample, but it is broadened. The spectra of the salts of both $U_{60}Ox_{30}$ and $U_{24}Pp_{12}$ clusters exhibit

DOI: 10.1021/acs.inorgchem.9b02132
Inorg. Chem. 2019, 58, 14112−14119

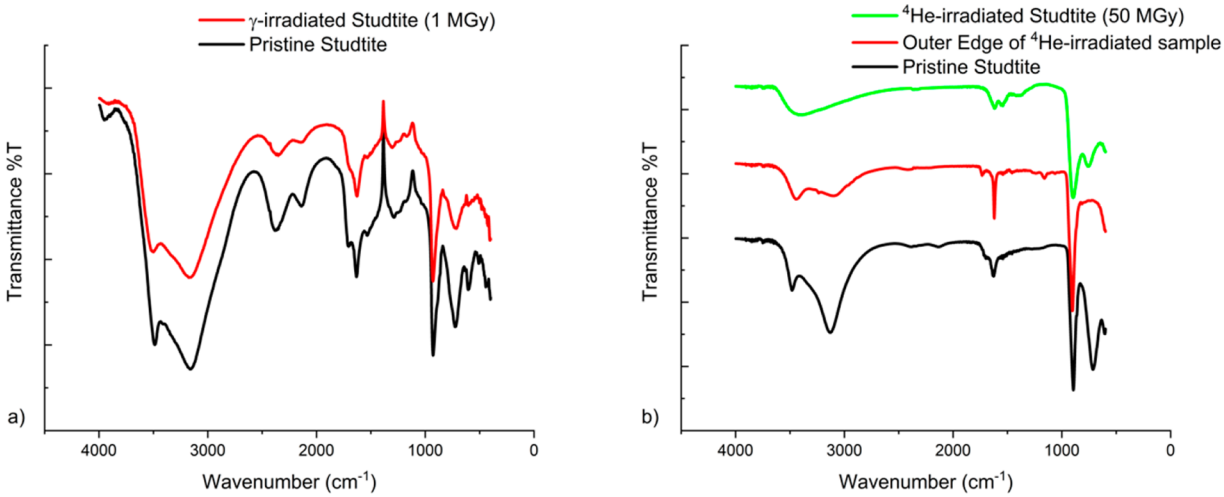

Figure 4. Infrared spectra of studtite (a) before irradiation and after γ-irradiation and (b) before and after He-irradiation.

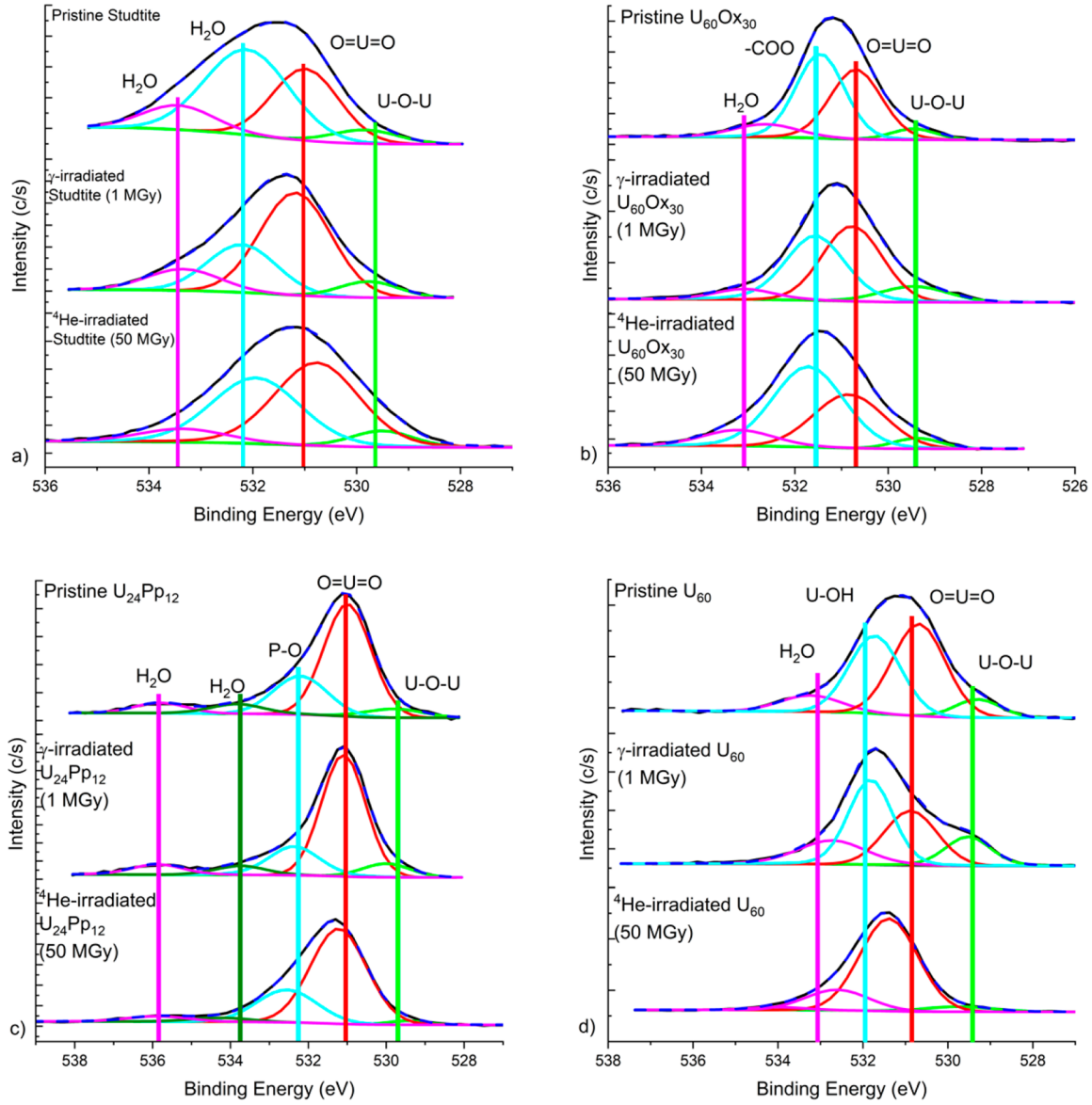

Figure 5. Oxygen XPS envelopes for (a) studtite, (b) $U_{60}Ox_{30}$ salt, (c) $U_{24}Pp_{12}$ salt, and (d) U_{60} salt with the raw data represented by a black line and the summed fit by a dotted blue line. Each peak is labeled with the corresponding oxygen.

DOI: 10.1021/acs.inorgchem.9b02132
Inorg. Chem. 2019, 58, 14112−14119

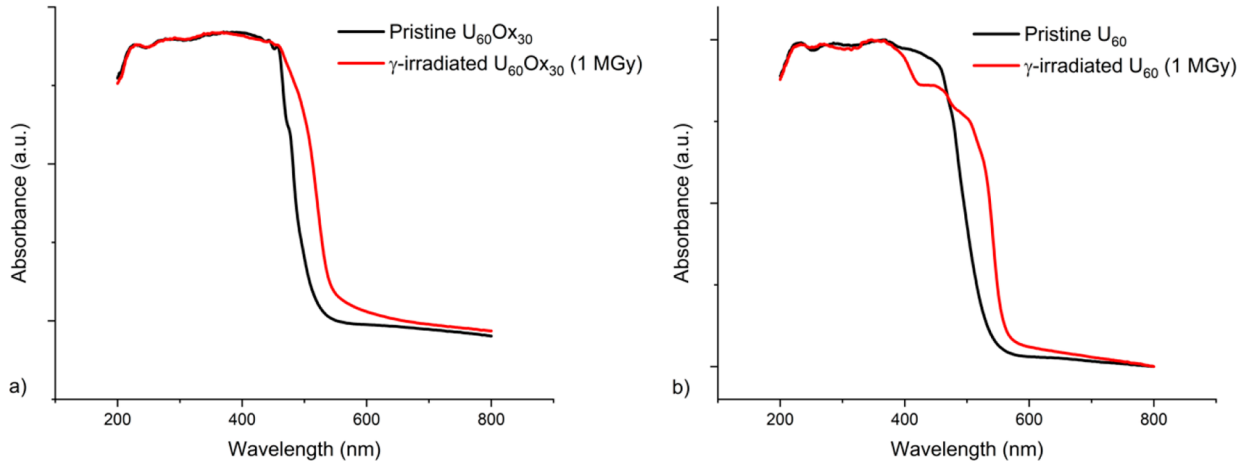

Figure 6. UV−vis of (a) $U_{60}Ox_{30}$ and (b) U_{60} showing the color change from yellow to orange.

broadening of the peaks due to He ion irradiation, but also a small additional peak appears at 747 and 758 cm^{-1}, respectively. The spectra of all He ion irradiated samples exhibit varying degrees of formation of a new Raman peak at approximately 750 cm^{-1} indicating the breakdown of the uranyl peroxide compounds due to He ion irradiation. The Raman spectroscopy extended scans are given in Supporting Information (Figures S1−S4).

Infrared spectra were collected for each sample under study to further characterize any changes in the chemical composition due to radiation effects. The spectrum of studtite has two broad bands from 3500 to 3000 cm^{-1} due to the −OH stretch (Figure 4). The peak at approximately 1700 cm^{-1} is also from the −OH stretch while the peak around 1630 cm^{-1} is due to the bending mode of H_2O molecules. The stretches at 915 and 750 cm^{-1} are assigned as the uranyl (U═O) asymmetric and symmetric vibrations, respectively.[39−42] The asymmetric stretch of the bridging peroxo group (U−O) appears at approximately 600 cm^{-1}.[37] The salt of $U_{60}Ox_{30}$ infrared spectrum (Figure S5a) has similar features with additional peaks between 1600 and 1300 cm^{-1} (C−O) from the oxalate ligand. The IR spectra of the salts of $U_{24}Pp_{12}$ and U_{60} have similar features arising from the uranyl and bridging peroxo as previously described (Figures S6a and S7a). The spectrum of the salt of $U_{24}Pp_{12}$ has four additional peaks from the pyrophosphate groups located between 980 and 1170 cm^{-1}. All analyzed spectra display no major changes before and after 1 MGy γ-irradiation. For He ion irradiation, slight changes are visible in the IR spectra. The spectrum for studtite reflects the conversion to metastudtite during the irradiation process,[17] but the peaks due to absorbed H_2O and the symmetric and antisymmetric stretching of the uranyl ions remain in the spectrum of the He ion irradiated sample (Figure 4b). The He ion irradiated sample of the $U_{60}Ox_{30}$ salt shows major shifts in the region assigned to the oxalate ligand from 1600 to 1300 cm^{-1} indicating that the oxalate ligand is affected by α-irradiation (Figure S5b). The spectra of the salts of $U_{24}Pp_{12}$ and U_{60} show very little change after 50 MGy He ion irradiation (Figures S6b and S7b).

High-resolution XPS scans were used to examine the U $4f_{7/2}$, U $4f_{5/2}$, and O 1s envelopes upon radiolysis of the uranyl peroxide compounds under study. Spectra for both U $4f_{7/2}$ and U $4f_{5/2}$ of all of the compounds are given in the Supporting Information Figures S8−S11. Both U 4f envelopes exhibit no major changes before and after γ-irradiation to 1 MGy. The O 1s envelope reflects all of the bonds between oxygen and uranium and provides additional information about the sample. The peaks were assigned using previously reported XPS data from uranyl minerals and synthetic compounds.[43,44] The binding energy (eV) ranges differ slightly for the salts of the large uranyl peroxide clusters compared to the uranyl minerals. All of the uranyl peroxide compounds contain a band resulting from the O atoms linking uranyl polyhedra (U−O−U) and the uranyl (O═U═O). The four main bands observed for studtite in Figure 5a were assigned to O atoms bridging uranyl polyhedra (U−O−U), uranyl (O═U═O), and two types of H_2O molecules. The same bonding types are present within the spectra of the salt of $U_{60}Ox_{30}$ and include the addition of carboxyl (COO) groups associated with the oxalate ligand (Figure 5b). For the salt of the $U_{24}Pp_{12}$ cluster, the spectrum includes signals from the P−O bond within the pyrophosphate ligand, in addition to the uranyl, bridging O atoms, and H_2O molecules (Figure 5c). The U_{60} cluster has the bridging O atoms, uranyl, and H_2O bands present with the addition of the hydroxyl (OH) group bound to the equatorial position of the uranyl hexagonal bipyramids in the structure (Figure 5d). Upon analysis of the O 1s envelopes of the spectra of studtite, $U_{60}Ox_{30}$ salt, and $U_{24}Pp_{12}$ salt, very little variation occurs in the location or area of the peaks before and after 1 MGy γ-irradiation. The spectrum of U_{60} salt exhibits a decrease in the area of the uranyl band, in agreement with the conclusion from the Raman spectra that the uranyl bond is affected by γ-irradiation. For He ion irradiation, small changes are visible in each O 1s spectral envelope. For the salt of $U_{24}Pp_{12}$, the spectral U−O−U peak has slightly decreased. The largest difference is for the salt of U_{60} (Figure 5d), as the band we associated with U−OH bonds is absent in the He ion irradiated sample. In addition, the peaks are shifted slightly, perhaps due to the breakdown of U_{60}. The U 4f envelopes do not exhibit major changes except for the spectrum of the salt of $U_{24}Pp_{12}$ in which a new peak in the binding energy range for U^{5+} and U^{4+} is present in the He ion irradiated U $4f_{7/2}$ envelope (Figure S10). Production of U^{4+} or U^{5+} from U^{6+} along with phase modification has been shown to occur with irradiation.[45] XPS is a surface sensitive technique and is not descriptive of the bulk material.

The salts of both $U_{60}Ox_{30}$ and U_{60} change from bright yellow to orange during γ-irradiation. UV−vis spectra exhibit a

DOI: 10.1021/acs.inorgchem.9b02132
Inorg. Chem. 2019, 58, 14112−14119

corresponding shift in Figure 6. For reference, the UV−vis spectra of studtite and $U_{24}Pp_{12}$ are given in Figures S12 and S13, respectively. We propose that the color change is due to modification of the chemical environment of the uranyl bond, as also indicated in the Raman and XPS spectra. Similar color changes occur upon formation of a uranyl dimeric cluster by incorporating a peroxo group in the equatorial plane of the hexagonal bipyramid.[46] During irradiation, a change in bandgap can also occur due to trapped electrons. Electrons could induce a stronger cation−uranyl interaction when they are ejected by the irradiation, leading to a weaker uranyl bond. Both of these phenomena are potential reasons for the elongation of the uranyl bond and change in the bandgap.

Under He ion irradiation the color of studtite and the salt of U_{60} changes (Figure 7). Upon addition of liquid water to

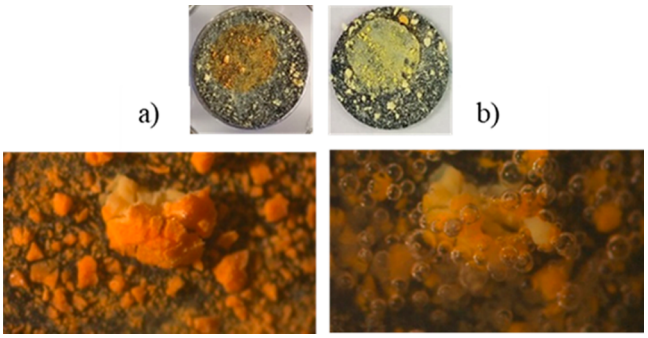

Figure 7. Water reaction with He ion irradiated studtite (a) prior to addition of water and (b) after addition of water.

irradiated material, an immediate reaction occurs that releases a gas (most likely O_2) attributed to the breakdown of peroxide (Figure 7 and Figure S14). Addition of water to the He ion irradiated studtite caused conversion to bright yellow uranyl oxide hydrate, metaschoepite, as shown by Raman and PXRD in Figures S15 and S16, respectively. The pristine salt of U_{60} readily dissolved in H_2O whereas the irradiated material reacted with water releasing O_2 gas. Most uranium oxides are unreactive with water; therefore, this reactivity is most likely due to a strained uranyl configuration. Similar properties have been reported for U_2O_7, an amorphous uranyl peroxide material found in yellowcake and formed from the heating of studtite at 200 °C for 4 h. The proposed structure of U_2O_7 is two bent uranyl ions bridged by a parallel bidentate peroxide group and O atom.[17] The breakdown of both studtite and the salt of U_{60} results in an amorphous uranyl peroxide that is most likely a smaller species similar to U_2O_7.

CONCLUSIONS

The responses of a variety of solid uranyl peroxide compounds with different structure topologies to intense γ-irradiation and He ion irradiation were characterized. All uranyl compounds studied show a reduction of crystallinity with intense γ-irradiation. The salt of U_{60} responds the most to γ-irradiation. The red-shift of the uranyl stretch in the corresponding Raman spectrum indicates weakening of the uranyl bond potentially due to addition of stronger equatorial bonds or cation−uranyl interaction produced by an ejected electron. This shift along with the additional decrease in the uranyl band of the XPS suggests some breakdown of the U_{60} cluster in the solid form under γ-irradiation. Studtite, $U_{60}Ox_{30}$ salt, and $U_{24}Pp_{12}$ salt are relatively stable with regards to direct γ-radiolysis. Under He ion irradiation, all compounds tested produced a new Raman spectral peak at approximately 750 cm^{-1} indicating their breakdown and the formation of at least one new species. Studtite and U_{60} salt were the most impacted by the He ion irradiation. The product formed by He ion irradiation was determined to be an amorphous uranyl peroxide phase by PXRD, which is likely a smaller species similar to previously described U_2O_7. Future studies are ongoing to decipher the structure of the uranyl peroxide produced by He ion irradiation. These results may lead the way to understanding the effects of radiation on uranyl peroxide compounds under different environmental conditions.

ASSOCIATED CONTENT

Supporting Information

The Supporting Information is available free of charge on the ACS Publications website at DOI: 10.1021/acs.inorgchem.9b02132.

Raman spectroscopy, infrared spectroscopy, X-ray photoelectron spectroscopy, UV−vis spectra, sample images, powder X-ray diffraction, and Raman spectroscopy fitting parameters (PDF)

AUTHOR INFORMATION

Corresponding Author

*E-mail: Jay.A.LaVerne.1@nd.edu.

ORCID

Peter C. Burns: 0000-0002-2319-9628

Jay A. LaVerne: 0000-0002-8383-7476

Author Contributions

The manuscript was written through contributions of all authors. All authors have given approval to the final version of the manuscript.

Funding

This research was supported by Department of Energy, National Nuclear Security Administration, under Award Number DE-NA0003763.

Notes

The authors declare no competing financial interest.

ACKNOWLEDGMENTS

The authors thank Hrafn Traustason for synthetic contributions by providing uranyl peroxide compounds. The authors acknowledge the Center for Sustainable Energy at Notre Dame (ND Energy) Materials Characterization Facilities for the use of the PHI VersaProble II X-ray photoelectron spectrometer, Jasco V-670 UV−vis−NIR spectrometer, and Bruker D8 Advance Davinci powder X-ray diffractometer. Support of the National Science Foundation through MRI award 1126374 is acknowledged for the XPS data in this paper. The authors thank Prof. Michael Wiescher for making available the facilities of the Notre Dame Nuclear Science Laboratory, which is supported by the U.S. National Science Foundation through Grant Phys-0758100, and Prof. Ian Carmichael for making available the facilities of the Notre Dame Radiation Laboratory, which is supported by DOE BES through Grant DE-FC02-04ER15533. This contribution is NDRL-5252 from the Notre Dame Radiation Laboratory.

DOI: 10.1021/acs.inorgchem.9b02132
Inorg. Chem. 2019, 58, 14112−14119

REFERENCES

(1) Hanson, B.; McNamara, B.; Buck, E.; Friese, J.; Jenson, E.; Krupka, K.; Arey, B. Corrosion of commercial spent nuclear fuel. 1. Formation of studtite and metastudtite. *Radiochim. Acta* **2005**, *93*, 159−168.

(2) Hickam, S.; Breier, J.; Cripe, Y.; Cole, E.; Burns, P. C. Effects of H_2O_2 Concentration on Formation of Uranyl Peroxide Species Probed by Dissolution of Uranium Nitride and Uranium Dioxide. *Inorg. Chem.* **2019**, *58*, 5858−5864.

(3) McNamara, B.; Hanson, B.; Buck, E.; Soderquist, C. Corrosion of commercial spent nuclear fuel. 2. Radiochemical analyses of metastudtite and leachates. *Radiochim. Acta* **2005**, *93*, 169−175.

(4) Nyman, M.; Burns, P. C. A comprehensive comparison of transition-metal and actinyl polyoxometalates. *Chem. Soc. Rev.* **2012**, *41*, 7354−7367.

(5) Kubatko, K.-A. H.; Helean, K. B.; Navrotsky, A.; Burns, P. C. Stability of Peroxide-Containing Uranyl Minerals. *Science* **2003**, *302*, 1191−1193.

(6) Burns, P. C.; Kubatko, K.-A.; Sigmon, G.; Fryer, B. J.; Gagnon, J. E.; Antonio, M. R.; Soderholm, L. Actinyl Peroxide Nanospheres. *Angew. Chem., Int. Ed.* **2005**, *44*, 2135−2139.

(7) Burns, P. C.; Nyman, M. Captivation with encapsulation: a dozen years of exploring uranyl peroxide capsules. *Dalton Trans.* **2018**, *47*, 5916−5927.

(8) Qiu, J.; Burns, P. C. Clusters of Actinides with Oxide, Peroxide, or Hydroxide Bridges. *Chem. Rev.* **2013**, *113*, 1097−1120.

(9) Armstrong, C. R.; Nyman, M.; Shvareva, T.; Sigmon, G. E.; Burns, P. C.; Navrotsky, A. Uranyl peroxide enhanced nuclear fuel corrosion in seawater. *Proc. Natl. Acad. Sci. U. S. A.* **2012**, *109*, 1874−1877.

(10) Wylie, E. M.; Peruski, K. M.; Prizio, S. E.; Bridges, A. N. A.; Rudisill, T. S.; Hobbs, D. T.; Phillip, W. A.; Burns, P. C. Processing used nuclear fuel with nanoscale control of uranium and ultrafiltration. *J. Nucl. Mater.* **2016**, *473*, 125−130.

(11) Wylie, E. M.; Peruski, K. M.; Weidman, J. L.; Phillip, W. A.; Burns, P. C. Ultrafiltration of Uranyl Peroxide Nanoclusters for the Separation of Uranium from Aqueous Solution. *ACS Appl. Mater. Interfaces* **2014**, *6*, 473−479.

(12) Fairley, T. I. Study of hydrogen dioxide and certain peroxides, including experiment to determine the heat of formation of the oxygen-molecule. *J. Chem. Soc.* **1877**, *31*, 1−24.

(13) Watt, G. W.; Achorn, S. L.; Marley, J. L. Some chemical and physical properties of uranium peroxide. *J. Am. Chem. Soc.* **1950**, *72*, 3341−3343.

(14) Burns, P. C.; Hughes, K.-A. Studtite, $[(UO_2)(O_2)(H_2O)_2]$-$(H_2O)_2$: The first structure of a peroxide mineral. *Am. Mineral.* **2003**, *88*, 1165−1168.

(15) Vaes, J. F. Six nouveaux mineraux d'urane provenant de Shinkolobwe (Katanga). *Soc. Geol. Belgique Ann.* **1947**, *70*, B212−B229.

(16) Deliens, M.; Piret, P. Metastudtite, $UO_4.2H_2O$, a new mineral from Shinkolobwe, Shaba, Zaire. *Am. Mineral.* **1983**, *68*, 456−458.

(17) Odoh, S. O.; Shamblin, J.; Colla, C. A.; Hickam, S.; Lobeck, H. L.; Lopez, R. A. K.; Olds, T.; Szymanowski, J. E. S.; Sigmon, G. E.; Neuefeind, J.; Casey, W. H.; Lang, M.; Gagliardi, L.; Burns, P. C. Structure and Reactivity of X-ray Amorphous Uranyl Peroxide, U_2O_7. *Inorg. Chem.* **2016**, *55*, 3541−3546.

(18) Guo, X. F.; Wu, D.; Xu, H. W.; Burns, P. C.; Navrotsky, A. Thermodynamic studies of studtite thermal decomposition pathways via amorphous intermediates UO_3, U_2O_7, and UO_4. *J. Nucl. Mater.* **2016**, *478*, 158−163.

(19) *Root Cause Analysis Report September 9, 2014 Incident Investigation Pressurized Drum of Yellowcake at the Honeywell Uranium Refinery*; Golder Associates Inc., 2015. https://www.nrc.gov/docs/ML1508/ML15089A443.pdf (accessed Sep 26, 2019).

(20) Rey, A.; Casas, I.; Gimeńez, J.; de Pablo, J.; Ewing, R. C.; Utsunomiya, S. Stability of uranium (VI) peroxide hydrates under ionizing radiation. *Am. Mineral.* **2009**, *94*, 229−235.

(21) Falaise, C.; Nyman, M. The Key Role of U_{28} in the Aqueous Self-Assembly of Uranyl Peroxide Nanocages. *Chem. - Eur. J.* **2016**, *22*, 14678−14687.

(22) Flynn, S. L.; Szymanowski, J. E. S.; Gao, Y. Y.; Liu, T. B.; Burns, P. C.; Fein, J. B. Experimental measurements of U_{60} nanocluster stability in aqueous solution. *Geochim. Cosmochim. Acta* **2015**, *156*, 94−105.

(23) Sigmon, G. E.; Unruh, D. K.; Ling, J.; Weaver, B.; Ward, M.; Pressprich, L.; Simonetti, A.; Burns, P. C. Symmetry versus Minimal Pentagonal Adjacencies in Uranium-Based Polyoxometalate Fullerene Topologies. *Angew. Chem., Int. Ed.* **2009**, *48*, 2737−2740.

(24) Soltis, J. A.; Wallace, C. M.; Penn, R. L.; Burns, P. C. Cation-Dependent Hierarchical Assembly of U_{60} Nanoclusters into Macro-Ion Assemblies Imaged via Cryogenic Transmission Electron Microscopy. *J. Am. Chem. Soc.* **2016**, *138*, 191−198.

(25) Yu, Q.; Fein, J. B. Enzymatic reduction of U_{60} nanoclusters by Shewanella oneidensis MR-1. *Radiochim. Acta* **2018**, *106*, 21−30.

(26) Turner, K. M.; Szymanowski, J. E. S.; Zhang, F.; Lin, Y.; McGrail, B. T.; Mao, W. L.; Burns, P. C.; Ewing, R. C. Uranyl peroxide nanoclusters at high-pressure. *J. Mater. Res.* **2017**, *32*, 3679−3688.

(27) Sadergaski, L. R.; Hixon, A. E. Kinetics of Uranyl Peroxide Nanocluster (U_{60}) Sorption to Goethite. *Environ. Sci. Technol.* **2018**, *52*, 9818−9826.

(28) Sadergaski, L. R.; Stoxen, W.; Hixon, A. E. Uranyl Peroxide Nanocluster (U_{60}) Persistence and Sorption in the Presence of Hematite. *Environ. Sci. Technol.* **2018**, *52*, 3304−3311.

(29) Ling, J.; Qiu, J.; Burns, P. C. Uranyl Peroxide Oxalate Cage and Core−Shell Clusters Containing 50 and 120 Uranyl Ions. *Inorg. Chem.* **2012**, *51*, 2403−2408.

(30) Ling, J.; Wallace, C. M.; Szymanowski, J. E. S.; Burns, P. C. Hybrid Uranium−Oxalate Fullerene Topology Cage Clusters. *Angew. Chem., Int. Ed.* **2010**, *49*, 7271−7273.

(31) Lobeck, H. L.; Traustason, H.; Julien, P. A.; FitzPatrick, J. R.; Mana, S.; Szymanowski, J. E. S.; Burns, P. C. In situ Raman spectroscopy of uranyl peroxide nanoscale cage clusters under hydrothermal conditions. *Dalton Trans.* **2019**, *48*, 7755−7765.

(32) Dembowski, M.; Colla, C. A.; Hickam, S.; Oliveri, A. F.; Szymanowski, J. E. S.; Oliver, A. G.; Casey, W. H.; Burns, P. C. Hierarchy of Pyrophosphate-Functionalized Uranyl Peroxide Nanocluster Synthesis. *Inorg. Chem.* **2017**, *56*, 5478−5487.

(33) Ling, J.; Qiu, J.; Szymanowski, J. E. S.; Burns, P. C. Low-Symmetry Uranyl Pyrophosphate Cage Clusters. *Chem. - Eur. J.* **2011**, *17*, 2571−2574.

(34) Dembowski, M.; Olds, T. A.; Pellegrini, K. L.; Hoffmann, C.; Wang, X.; Hickam, S.; He, J.; Oliver, A. G.; Burns, P. C. Solution ^{31}P NMR Study of the Acid-Catalyzed Formation of a Highly Charged $\{U_{24}Pp_{12}\}$ Nanocluster, $[(UO_2)_{24}(O_2)_{24}(P_2O_7)_{12}]^{48-}$, and Its Structural Characterization in the Solid State Using Single-Crystal Neutron Diffraction. *J. Am. Chem. Soc.* **2016**, *138*, 8547−8553.

(35) Lu, G.; Haes, A. J.; Forbes, T. Z. Detection and identification of solids, surfaces, and solutions of uranium using vibrational spectroscopy. *Coord. Chem. Rev.* **2018**, *374*, 314−344.

(36) McGrail, B. T.; Sigmon, G. E.; Jouffret, L. J.; Andrews, C. R.; Burns, P. C. Raman Spectroscopic and ESI-MS Characterization of Uranyl Peroxide Cage Clusters. *Inorg. Chem.* **2014**, *53*, 1562−1569.

(37) Bastians, S.; Crump, G.; Griffith, W. P.; Withnall, R. Raspite and studtite: Raman spectra of two unique minerals. *J. Raman Spectrosc.* **2004**, *35*, 726−731.

(38) Tsushima, S. On the "yl" bond weakening in uranyl(VI) coordination complexes. *Dalton Trans.* **2011**, *40*, 6732−6737.

(39) Sato, T. Thermal decomposition of uranium peroxide hydrates. *J. Appl. Chem. Biotechnol.* **1976**, *26*, 207−213.

(40) Cejka, J.; Sejkora, J.; Deliens, M. New data on studtite, $UO_4 \cdot 4H_2O$, from Shinkolobwe, Shaba, Zaire. *Neues Jahrb. Mineral., Monatsh.* **1996**, 125−134.

(41) Rocchiccioli, C. Etude par thermogravimetrie analyse thermique differentielle et spectrographie dabsorption infrarouge

DOI: 10.1021/acs.inorgchem.9b02132
Inorg. Chem. 2019, 58, 14112−14119

des hydrates du peroxyde duranium. *C. R. Hebd. Seances Acad. Sci.* **1966**, *263*, 1061−1066.
(42) Čejka, J. Infrared spectroscopy and thermal analysis of the uranyl minerals. *Rev. Mineral.* **1999**, *38*, 521−622.
(43) Schindler, M.; Hawthorne, F. C.; Freund, M. S.; Burns, P. C. XPS spectra of uranyl minerals and synthetic uranyl compounds. I: The U 4f spectrum. *Geochim. Cosmochim. Acta* **2009**, *73*, 2471−2487.
(44) Schindler, M.; Hawthorne, F. C.; Freund, M. S.; Burns, P. C. XPS spectra of uranyl minerals and synthetic uranyl compounds. II: The O 1s spectrum. *Geochim. Cosmochim. Acta* **2009**, *73*, 2488−2509.
(45) Tracy, C. L.; Lang, M.; Pray, J. M.; Zhang, F.; Popov, D.; Park, C.; Trautmann, C.; Bender, M.; Severin, D.; Skuratov, V. A.; Ewing, R. C. Redox response of actinide materials to highly ionizing radiation. *Nat. Commun.* **2015**, *6*, 6133.
(46) Jayasinghe, A. S.; Applegate, L. C.; Unruh, D. K.; Hutton, J.; Forbes, T. Z. Utilizing Autoxidation of Solvents To Promote the Formation of Uranyl Peroxide Materials. *Cryst. Growth Des.* **2019**, *19*, 1756−1766.

DOI: 10.1021/acs.inorgchem.9b02132
Inorg. Chem. 2019, 58, 14112−14119